Journal of Nuclear Materials 414 (2011) 53–68

Contents lists available at ScienceDirect

Journal of Nuclear Materials

journal homepage: www.elsevier.com/locate/jnucmat

Assessment of design limits and criteria requirements for Eurofer structures in TBM components

G. Aiello [a,*], J. Aktaa [b], F. Cismondi [c], G. Rampal [a], J.-F. Salavy [a], F. Tavassoli [d]

[a] CEA, DEN/DANS/DM2S, F-91191 Gif-sur-Yvette, France
[b] Forschungszentrum Karlsruhe (FZK), Institute for Materials Research II, Hermann-von-Helmholtz-Platz 1, 76344 Eggenstein-Leopoldshafen, Germany
[c] Forschungszentrum Karlsruhe (FZK), Institut für Neutronenphysik und Reaktortechnik, Hermann-von-Helmholtz-Platz 1, 76344 Eggenstein-Leopoldshafen, Germany
[d] CEA, DEN/DANS/DMN/DIR, F-91191 Gif-sur-Yvette, France

ARTICLE INFO

Article history:
Received 1 September 2010
Accepted 3 May 2011
Available online 7 May 2011

ABSTRACT

Eurofer97 is a Reduced Activation Ferritic-Martensitic (RAFM) steel developed for use as structural material in fusion power reactors blankets and in particular the future DEMOnstration power plant that should follow ITER. In order to evaluate the performances of the different blanket concepts in a fusion-relevant environment, the ITER experimental programme foresees the installation of dedicated Test Blanket Modules (TBMs), representative of the corresponding DEMO blankets, in selected equatorial ports. To be fully relevant, TBMs will have to be designed and fabricated using DEMO relevant technologies and will, in particular, use Eurofer97 as structural material.

While the use of ferritic/martensitic steels is not new in the nuclear industry, the fusion environment in ITER poses new challenges for the structural materials. Besides, contrary to DEMO, ITER is characterised by a strongly pulsed mode of operation that could have severe consequences on the lifetime of the components. This paper gives an overview of the issues related to the design of Eurofer97 structures in TBM components, discussing the choice of reference Codes&Standards and the consistency of the design rules with Eurofer97 mechanical properties.

© 2011 Elsevier B.V. All rights reserved.

1. Introduction

One of the main technological barriers to the design of tritium breeding blankets for fusion power systems is the development of structural materials capable of withstanding complex thermo-mechanical loadings and high-energy neutron irradiation while presenting at the same time low-activation properties. Within the European Union, several blanket concepts have been investigated in the framework of the Power Plant Conceptual Study (PPCS) [1]. Since one decade, the EU follows the Helium Cooled Lithium Lead (HCLL) and the Helium Cooled Pebble Bed (HCPB) blankets as reference concepts for the future DEMOnstration power plant that should follow ITER [2]. Both blankets use a low activation 9%CrWVTa Reduced Activation Ferritic/Martensitic (RAFM) steel as structural material: Eurofer97 [3,4]. The ITER technological objectives [5] include that corresponding Test Blanket Modules (TBMs) could be installed in selected equatorial ports at the beginning of the hydrogen operation phase [6]. The EU strategy foresees to occupy one port with the two reference concepts to be tested. The EU aims to have TBMs designed and fabricated using DEMO relevant technologies and will, in particular, use Eurofer97 as structural material.

While the use of ferritic/martensitic steels is not new in the nuclear industry, the fusion environment in ITER poses new challenges for the structural materials [7,8]. Besides, contrary to DEMO, ITER is characterised by a strongly pulsed mode of operation that could have severe consequences on the lifetime of the components. The design of TBMs will therefore have to be based on a consistent set of rules taking into account, at the same time, regulation requirements for nuclear components, the peculiarities of Eurofer97 mechanical behaviour and the specific operating conditions inside the ITER environment. Each of these points is discussed in the following sections.

2. Choice of a reference design code for TBM components

In order to orient the choice of a design code for TBM components, several factors need to be considered:

– Safety classification: ITER, as the device operator, considers TBMs as non-Safety Important Components (non-SIC). The requirements in terms of safety only rely on the limitation

* Corresponding author. Tel.: +33 1 69086358; fax: +33 1 69089935.
E-mail address: giacomo.aiello@cea.fr (G. Aiello).

0022-3115/$ - see front matter © 2011 Elsevier B.V. All rights reserved.
doi:10.1016/j.jnucmat.2011.05.005

of the "hydrogen risk", by limiting the volumes of PbLi and Beryllium (for possible interaction with water). This can be solved by design.
- Investment protection: a high quality level is required, as well as a good quality assurance. This can be managed by specific provisions given in the codes concerning materials' procurement, manufacturing, assembling techniques and examination methods.
- Regulation requirements: since ITER will be built in France, TBMs must fulfil French and European regulations on (nuclear) pressure vessel equipments.

Among the existing French and European regulatory documents, those identified as establishing specific requirements for the design and manufacture of the HCLL and HCPB Test Blanket Systems (TBS) are:

- The Pressure Equipment Directive (PED – 97/23/EC) adopted by the European Parliament and European Council in May 1997 [9].
- The French Order dated 12th December 2005 concerning nuclear pressure equipment (Equipements Sous Pression Nucléaires – ESPN [10])
- The French Order concerning Quality of Design, Construction and Operation of Basis Nuclear Installations [11].

These basic regulatory documents define the principle of equipment classification, formulate the general Essential Safety Requirements (ESR) and the ways to fulfil these requirements from the legal (and sometimes technical) point of view. According to ESPN, Nuclear Pressure Equipments (NPE) are classified into three levels, from N1 to N3, in relation to the significance of the radioactive emissions possibly resulting from their failure, and in 5 categories according to the pressure hazard: Category 0, I, II, III and IV. On the basis of a preliminary evaluation, the TBMs belong to ESPN N2 level, Category IV.

The philosophy of the regulatory documents is to give the manufacturer of a given equipment the choice of the design and manufacturing code for the component (ESPN refers to 'professional guides'), but he shall demonstrate the conformity of the selected Code and Standards (C&S) with the ESR. In many cases, the conformity shall be assessed by a special third party organisation, so called Notified Body.

It is important to note that even when a code contains specific provisions to meet the ESR, its use does not automatically assure conformity with regulations: other factors, like the materials used and the component's operating conditions need to be taken into account. PED and ESPN, for example, define limit values for the mechanical and physical properties of the structural materials that can be used in the construction of (N)PEs. Concerning the operating conditions, plasma facing components in ITER have to withstand a combination of loads that are seldom, if ever, encountered in conventional (fission) nuclear power plants: the TBMs in particular experience a combination of high temperature, neutron irradiation and pulsed mode of operation. Design rules contained in the codes are intended to prevent failure resulting from specific damage modes, and the selected C&S shall cover all possible damage modes specific to TBMs. Each code has a domain of applicability, and it is to the designer to verify that a given component falls within this domain. In case of TBMs, the selected C&S should at least present the following features:

- Guidelines for conformity with PED and ESPN ESR.
- Design rules for high temperature operation.
- Design rules for irradiated materials.
- Consistency of design rules with Eurofer97 mechanical properties data and TBMs-specific manufacturing and joining techniques. Reference Procurement Specifications (RPS) providing the requirements for procurement of Eurofer97 parts and products shall also be included.

The last item is possibly optional, since certificates of conformity of a given material with the ESR can also be issued by the Notified Bodies at the request of the manufacturer of a (N)PE. Having a single C&S covering all of TBMs-specific features would however considerably simplify the task of the designer/manufacturer.

3. Review of available C&S for TBM components

The unique features of TBMs and more generally of the ITER environment are very unlikely to be covered by only one existing industrial code. A multi-code approach has then been applied for the selection of C&S for TBM components (Table 1). This is consistent with the approach used for ITER mechanical components [12].

For the design of in-vessel components, ITER recommends the use of the ASME Boiler and Pressure Vessel Code (BPVC) Section VIII, Division 2 integrated by ITER Structural Design Criteria for In-vessel Components (SDC-IC) [13,14]. SDC-IC was developed as a collaboration between the four ITER Parties of Europe, Japan, the Russian Federation and the United States in order to have a specific code covering all the features of plasma-facing components. In particular, SDC-IC contains specific rules to take into account the effects of irradiation on structural materials, which are not covered by the ASME BPVC. On the other hand, the scope of SDC-IC is currently limited to criteria related to design. Rules for manufacturing, quality assurance and examination are instead covered by ASME BPVC.

While this approach is sound for generic in-vessel components, it is more delicate in case of TBMs since they have to comply with ESPN regulation. ASME has published a guide explaining how to meet ESR defined by PED using BPVC Section VIII [15], but no specific guidelines are given to meet conformity with the ESPN order. Also, Eurofer97 is included neither in ASME nor in SDC-IC material data sections. Although a collection of Eurofer97 properties [16] has been produced in the context of the European Fusion Develop-

Table 1
Assessment of selected C&S features for TBMs design.

C&S	Conformity with PED	Conformity with ESPN	High temperature design rules	Irradiated materials design rules	Eurofer97 properties	Comments
ASME	Yes	No	Yes	No	No	
SDC-IC	No	No	Yes	Yes	No	Scope limited to design rules.
RCC-MR	Yes	Yes	Yes	No	No	
RCC-MX	Yes	Yes	Yes	Yes	No	Developed for internal use by CEA only
RCC-MRx	Yes	Yes	Yes	Yes	Possibly	Still in development

ment Agreement (EFDA) activities, Eurofer97 use as structural material in TBMs would need to be validated separately.

For these reasons, in past EU TBMs design activities[17,18], RCC-MR [19] has been considered as the reference design code for the TBM assembly instead of ASME. RCC-MR is the reference French code for high temperature reactors and the 2007 edition contains a specific appendix (A18) to cover PED and ESPN requirements. In fact, to insure compliance with the ESPN order of the ITER Vacuum Vessel, which is classified as a multi-chamber equipment with pressure Category IV and nuclear level N2 like TBMs, the ITER EU Domestic Agency asked for specific provisions to be included in RCC-MR (Appendix A19). Contrary to TBMs, however the level of neutron irradiation expected in the VV is such that neutron-irradiation effects on material properties are negligible (at least from the structural integrity point of view). Since RCC-MR does not cover measures to be taken to prevent damages resulting from irradiation, the use of SDC-IC was still necessary for TBMs. This approach however is still not satisfactory because:

- Design rules addressing the effects of irradiation in SDC-IC have been developed mainly for the 316L(N)-IG steel grade on which the design of the ITER blanket is based [14,20]. The mechanical properties of Eurofer97 are very different from those of austenitic steels. The validity/degree of conservatism of the rules defined in SDC-IC needs therefore to be verified for RAFM steels.
- Eurofer97 is included neither in RCC-MR nor in SDC-IC material data sections. As such, its use as structural material in NPEs still needs to be validated.

Concerning neutron-irradiation effects, a possible alternative to SDC-IC is RCC-MX [21], an extension of the RCC-MR code developed for internal use by CEA for fission experimental reactors, ancillary systems and irradiation rigs. Indeed, the next edition of RCC-MR, which will be called RCC-MRx, is expected to include RCC-MX specific rules for irradiated materials in order to have a single code suited for the design of all nuclear components to be operated in next generation reactors. Concerning the inclusion of Eurofer97 properties and specific manufacturing techniques, since RCC-MRx is still in development, the possibility is open to contribute to the RCC-MRx evolutions by change requests submitted to AFCEN and/or involvement in AFCEN working groups. Eurofer97 could in this case be included in the code, allowing the use of RCC-MRx as the sole code for the design and manufacturing of TBMs [22].

Since conceptual design activities for EU TBMs are entering their final phase (it is expected that installation of TBMs in ITER will start in 2019 – [23]), it is important to understand the implications for the designers of using a given set of C&S. Also, mechanical and physical properties of Eurofer97 being considerably different from those of austenitic steels and from those of other martensitic steels considered in the nuclear industry, it is possible that some of the rules contained in the codes will need to be reconsidered and/or adapted.

In the next sections, after recalling the main mechanical properties of Eurofer97, the design rules and corresponding stress limits contained in the aforementioned C&S (in particular SDC-IC and RCC-MX) will be discussed.

4. Eurofer97 mechanical properties

RAFM steels are derived from the conventional modified 9Cr–1Mo steel, but with the high activation elements (Mo, Nb, Ni, Cu and N) eliminated or replaced by their equivalent low activation elements (e.g. W, V and Ta). Their main advantages over austenitic stainless steels are related to the excellent dimensional stability (creep and swelling) under neutron irradiation [24]. In addition, they present lower coefficients of thermal expansion and higher coefficients of thermal conductivity at high temperatures: at 500 °C RAFM steels have a surface heat capability factor about 2.5 times higher than that of austenitic steels [8,25]. Development of RAFM steels has been the object of extensive cooperation between the different fusion parties; Eurofer97 is one of the variants developed in the European Union within the framework of the EFDA. Given the lack of data concerning this type of steel in present-day design codes, a characterisation program has been launched in the past years to address the short-term needs related to TBM design activities [26]. While the database of Eurofer97 mechanical properties is not yet up to par with that of more commonly used austenitic steels, the recent availability of additional data concerning fatigue, creep and irradiation induced changes in material properties have brought the characterisation of Eurofer97 at least to the level of other 9Cr steels included in nuclear design codes.

4.1. Tensile strength and ductility properties

Fig. 1 shows the evolution of the yield strength (S_y) and ultimate tensile strength (S_u) of Eurofer97 with temperature compared to those of the 316L(N)-IG steel. In the whole range of temperatures relevant for TBM operation, Eurofer97 exhibits a much lower strain hardening capability compared to 316L(N)-IG. In particular, at 500 °C (corresponding to the average operating temperature of the TBM First Wall in ITER) the ratio S_y/S_u is ~0.9 for Eurofer97 and ~0.3 for 316L(N)-IG.

The lack of strain-hardening capability is also evident in Fig. 2 which compares the uniform (ε_u) and total elongation at rupture (ε_t) for Eurofer97 and 316L(N)-IG: starting from 400 °C, the uniform elongation of Eurofer97 falls below 2%, a value below which elastic follow up effects become relevant [20]. Total elongation, on the other hand, remains high, with values close to 20% in the whole TBM operating temperature range.

To give an idea of the reduced ductility/strain-hardening capability of Eurofer97 with respect to 316L(N)-IG, Fig. 3 shows the schematized stress–strain curves for the two steels at 500 °C. According to the values of the uniform elongation, Eurofer97 could be considered as a semi-brittle or even brittle material even in the absence of irradiation damage [27].

4.1.1. Irradiated conditions

A considerable amount of data concerning the mechanical properties of Eurofer97 following neutron irradiation has been produced and is available in literature [28–37]. As reported by several sources, 300 °C is the most critical irradiation temperature in terms of hardening and loss of ductility for RAFM steels. At higher temperatures (>400 °C) recovery of irradiation damage takes place, and no hardening is observed above 500 °C. At 300 °C ($T_{irr} = T_{test}$), a very rapid increase of irradiation hardening with the displacement dose is observed and S_y and S_u almost merge. Extending the irradiation to higher doses seems to indicate that saturation occurs somewhere between 10 dpa and 20 dpa with saturation values [30,31,33] close to 1000 MPa.

Concerning ductility values, the elongation of Eurofer97 is severely reduced already at very small doses. Values of the uniform elongation as low as 0.2% have been reported after 1.5 dpa at 300 °C [32]. According to [30], saturation of the uniform elongation is already reached at ~0.7 dpa, with values consistently below 0.5%. The reduction of the total elongation seems instead to saturate around 10 dpa, with values close to 10% [31,33]. Even at high doses, thus, the material retains considerable ductility after necking, which is confirmed by the values of the reduction of area

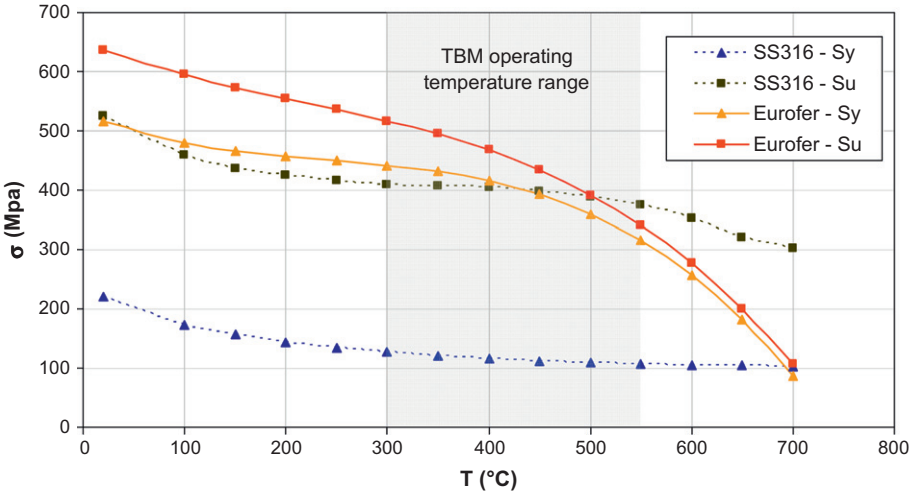

Fig. 1. Yield strength (S_y) and ultimate tensile strength (S_u) limits of Eurofer97 and 316L(N)-IG.

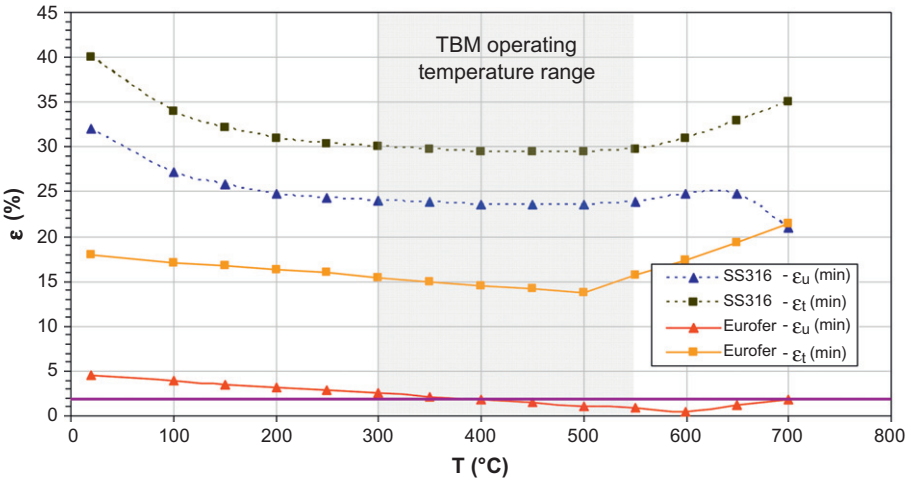

Fig. 2. Uniform elongation and total elongation values for Eurofer97 and 316L(N)-IG.

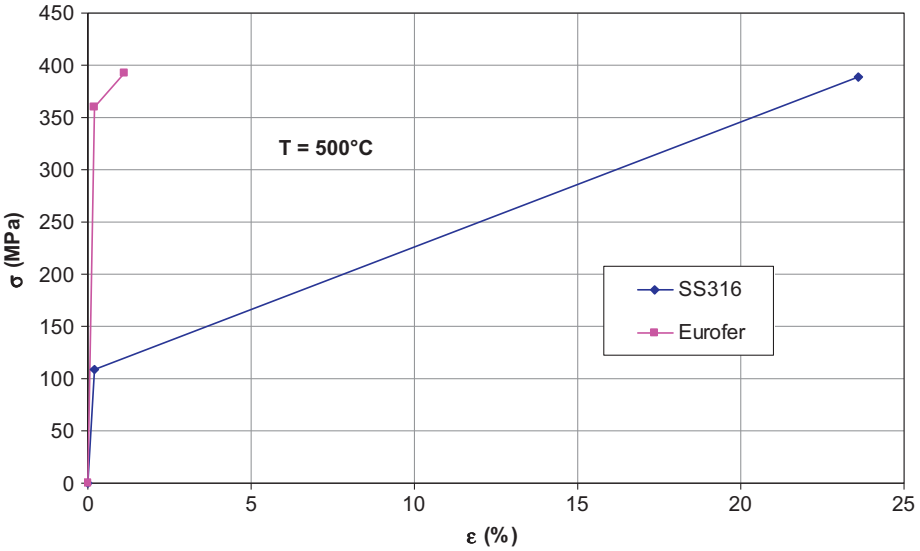

Fig. 3. Schematized stress–strain curve for Eurofer97 and 316L(N)-IG at 500 °C.

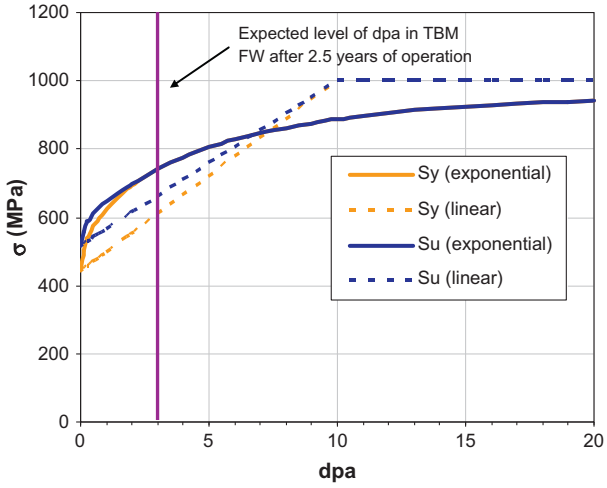

Fig. 4. Schematized evolution of S_y and S_u with the damage dose ($T = 300°$) for Eurofer97.

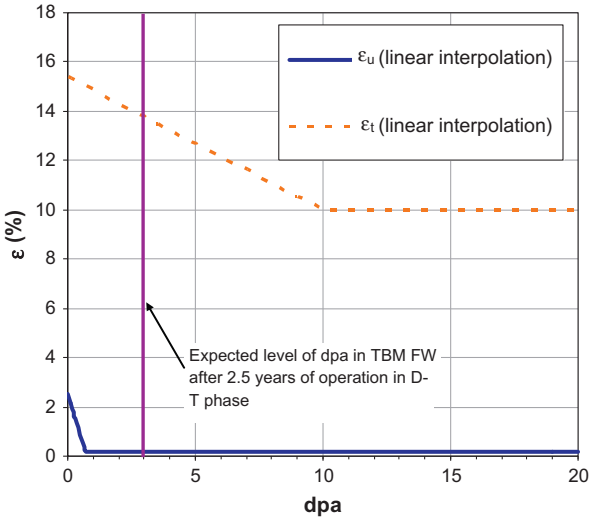

Fig. 5. Schematized evolution of ε_u and ε_t with the damage dose ($T = 300$ °C) for Eurofer97.

(%RA): values higher than 70% have been reported up to 10 dpa [30], and in excess of 50% up to 70 dpa [31].

In SDC-IC irradiation hardening is described by an exponential correlation of the form:

$$S^{irr} = S^{unirr} + a\sqrt{1 - \exp(-\phi/b)} \tag{1}$$

where ϕ is the dose in dpa, The 2008 edition of RCC-MX simplifies the construction of the curves describing the effect of irradiation by assuming a linear increase with dose until the saturation value:

$$S^{irr} = S^{unirr} + (S^{sat} - S^{unirr})\frac{D - D^0}{D^{sat} - D^0} \qquad (D^0 < D < D^{sat}) \tag{2}$$

where D is the damage dose (in dpa), S^{sat} and D^{sat} are respectively the strength at saturation and the saturation dose and D^0 is the dose below which effects of irradiation can be neglected.

Following the approach given in RCC-MX, Figs. 4 and 5 show respectively the evolutions of strength and elongation properties of Eurofer97 with the irradiation dose. Values of the coefficients in Eq. (2) have been conservatively inferred from data available in literature. The expected level of dpa in the TBM First Wall (FW) after 2.5 years of ITER operation is about 3 according to [38].

4.2. Thermal creep

The creep behaviour of Eurofer97 is well characterised with testing time of several experiments exceeding 10,000 h. Eurofer97 shows adequate creep rupture strength, comparable to that of other RAFM steels. Creep strain laws have been obtained and are available in the latest database of properties [16,26,39,40].

Starting from experimentally measured creep curves, the time dependent allowable stress intensity (S_t) is obtained as:

1. two thirds of the minimum stress corresponding to average creep rupture time t at temperature T;
2. 80% of the minimum stress corresponding to time t and temperature T for onset of tertiary creep;
3. minimum stress to cause a creep strain of min[1%, ε_c/5] in time t and temperature T, where ε_c is the minimum creep ductility.

Values of S_t for Eurofer97 are governed by 2/3 of the minimum stress to rupture and are shown in Fig. 6.

4.3. Fatigue properties

A considerable number of experimental results have recently been published concerning the fatigue behaviour of Eurofer97, especially in the Low Cycle Fatigue (LCF) regime which is of particular interest for the ITER environment [41–44].

Eurofer97, like all ferritic/martensitic steels, exhibit very pronounced softening under LCF tests: the cyclic stress amplitude decreases rapidly after a few cycles and then stabilizes at a value which decreases slowly as a function of the number of cycles, dropping sharply just before failure of the specimen. During fatigue tests, when saturation is reached, the range of the stable stress $\Delta\sigma$ can be plotted as a function of the imposed strain range $\Delta\varepsilon$. The curve thus determined is called the cyclic stress–strain curve. Cyclic stability is not achieved in LCF tests of Eurofer97: in this case, the cyclic stress–strain curves corresponding to half lives are reported as cyclic stress–strain curves. The coordinates ($\Delta\varepsilon$, $\Delta\sigma$) must be divided by 2 so that the cyclic stress–strain curves can be compared with the monotonic stress–strain curves (Fig. 7).

Starting from the results of fatigue tests, the total strain range is plotted against the number of cycles to failure in order to obtain the fatigue design curve, offsetting the mean experimental curves by a factor corresponding to the largest of the following cases (Fig. 8):

- division by 2 of the strain range,
- division by 20 of the number of cycles.

It should be stressed that these factors are intended to cover effects such as those of the environment, the scale (between the material and the test specimen) or the scattering of results. They in no case constitute a safety coefficient.

4.3.1. Effects of irradiation on fatigue behaviour

Few data are available on the consequences of neutron irradiation on the fatigue behaviour of Eurofer97 and other RAFM steels [45–47]. As a general rule, the fatigue lifetime of the irradiated material should be shorter because of loss of ductility and significant increase in cyclic softening. Experimental tests performed on Eurofer97 seem to indicate that this is the case in the high strain region of the fatigue curve ($\Delta\varepsilon > 1\%$), relevant for TBM design, where the decrease in N_f can be significant. In this case the material is loaded well above the yield stress point in the first cycle and no

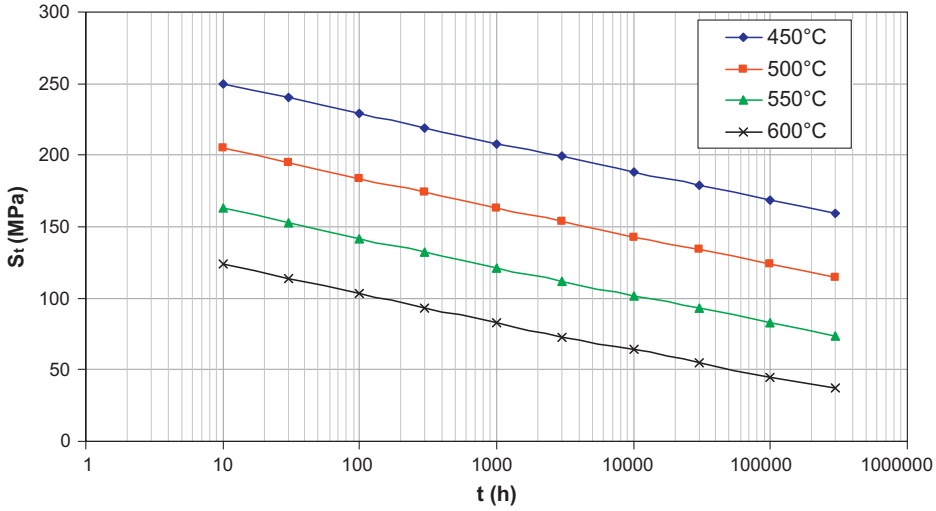

Fig. 6. Values of S_t for Eurofer 97 [16].

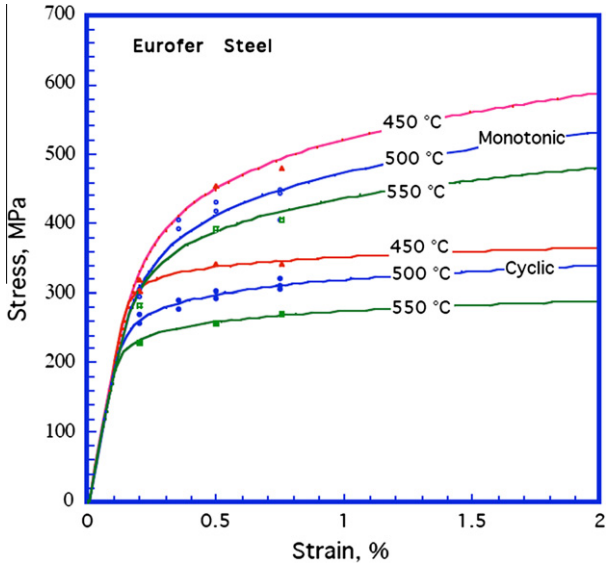

Fig. 7. Reduced cyclic stress–strain curves for Eurofer97 at different temperatures [16].

additional strain hardening takes place in subsequent cycles. This effect increases strongly with irradiation damage: more data are needed to assess its importance in the range of dpa expected for TBMs. For lower strain ranges, irradiation seems to have a positive effect, increasing the number of cycles to failure. This can be explained by the increase of the yield stress point (and consequently in the elastic range of the material) with irradiation hardening [45].

On the other hand, some results [48–51] seem to indicate that fatigue life can be considerably shorter than that of post-irradiated specimens when fatigue is imposed concurrently with irradiation. Post-irradiation experiments do not consider the fact that the microstructure of the material is changing during fatigue as well as during irradiation. Simultaneous irradiation and fatigue can develop a different microstructure and lead to different material response. This phenomenon is however highly dependant on the ratio between the dose rate and strain rate and more experimental tests are needed to assess its impact on the fatigue lifetime of TBMs in ITER.

4.4. Creep–fatigue interaction

TBM components will operate under cyclic, non-symmetrical thermo-mechanical loadings whose duration and intensities will depend on ITER operating parameters. In particular, TBMs will experience a quasi-stationary loading during the plasma pulse than can lead to creep damage accumulation. These operating conditions can be simulated by introducing a hold time in LCF tests. The fatigue behaviour of Eurofer97 becomes much more complicated when introducing hold times in LCF tests, showing very different characteristics with tension, compression or symmetrical hold times [41,52].

Experimental tests show that short hold times in tension (~500 s at 550 °C) at high strains have no negative (or even a positive) effect on the lifetime of the specimens (Fig. 9), which can be explained by the peak stress reduction because of the additional cyclic softening due to thermal creep. However, with longer hold times, creep damage increases and overcomes the beneficial effects of the additional cyclic softening, shortening the lifetime of the material. Similarly, at low strains, a reduction of the fatigue life is observed because, due to creep damage, the softening rate with hold times is much stronger, which corresponds to a large increase of the resulting plastic strain.

Hold time under compression, on the other hand, show a much a shorter lifetime (a factor of 2 or more) in comparison to the hold time under tension or even to hold time under tension and compression, regardless of the strain amplitude or hold time. This can be explained by the fact that hold time under compression does not cause a reduction of the tensile peak stress like hold time under tension does. This difference however seems to be related to the test environment: limited number of tests performed in vacuum show no difference between hold times in compression and in tension.

5. Treatment of irradiation effects in design codes

Beside changes in the mechanical properties, neutron irradiation causes additional creep and swelling of the material. Both SDC-IC and RCC-MX introduce additional criteria to take into account these phenomena, either in the form of additional design rules or by increasing the safety factors. SDC-IC states that, for 316L(N)-IG steel in ITER operating conditions, irradiation-induced creep and swelling are not of concern, while changes in the mechanical properties become relevant starting from 7 dpa.

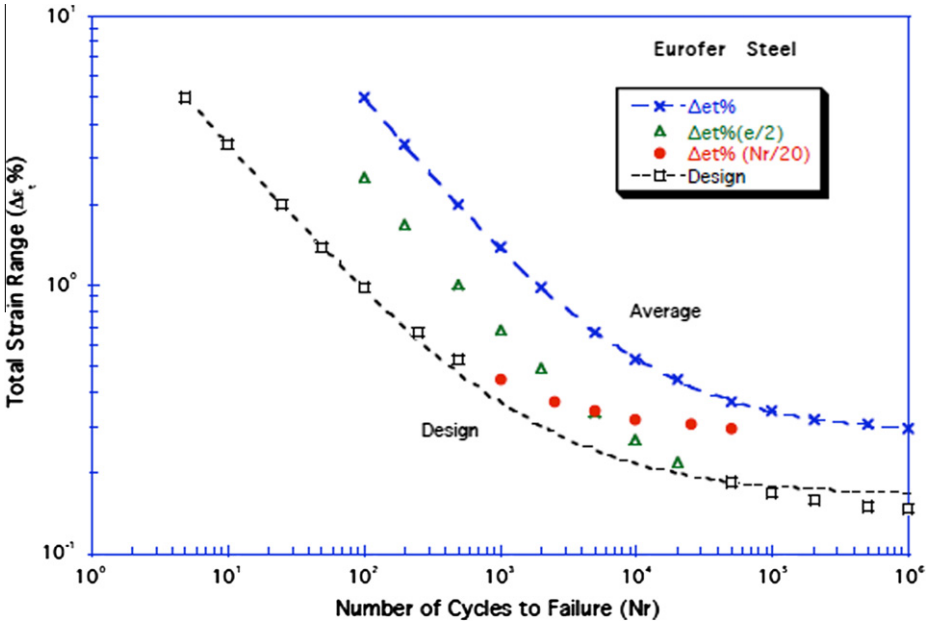

Fig. 8. Fatigue design curve of Eurofer97 [16].

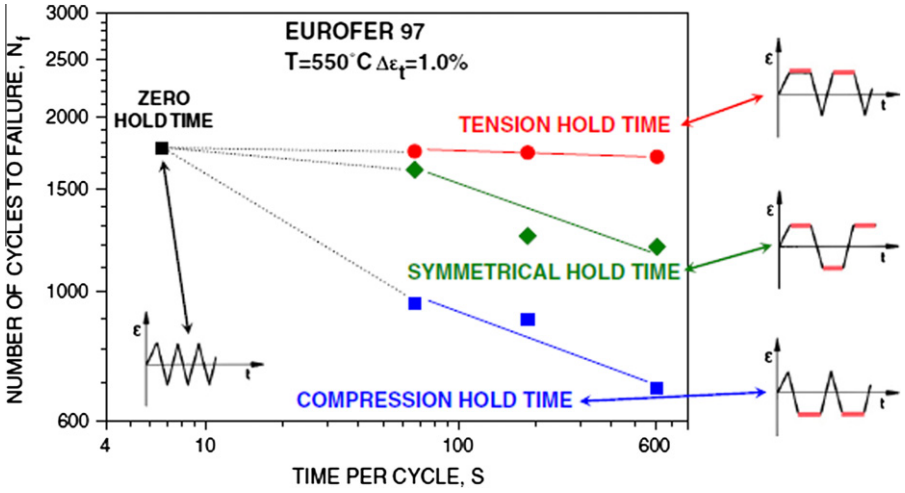

Fig. 9. Influence of hold times on the fatigue life of Eurofer97 [52].

Irradiation-induced creep and swelling can also be neglected in case of Eurofer97, as is to be expected since ferritic/martensitic steels show a much better resistance to these phenomena than austenitic steels. Changes in material properties (i.e. embrittlement and loss of strain-hardening) are instead a concern even at very low irradiation doses. In fact, criteria defined in SDC-IC take no advantage on the residual ductility of the material when the uniform elongation falls below 2%. For 316L(N)-IG steel, this corresponds to level of irradiation above 7 dpa. For $T = 300$ °C, the uniform elongation of Eurofer97 falls below 0.5% already at 0.7 dpa, and, for $T > 400$ °C, is lower than 2% even in unirradiated conditions (Beginning Of Life – BOL). Therefore, even if irradiation does not seem to affect significantly the ductility of the material for $T > 400$ °C, the BOL ductility properties are already sufficiently low to justify the use of adequate rules for the design of the components.

It should be recalled that ESPN defines minimum allowable values for the properties related to the ductility of the materials used in the construction of NPEs. These limits are not considered in SDC-IC, but they are in RCC-MX (Table 2). Eurofer97 meets these requirements at BOL but not in the irradiated conditions foreseen in TBMs. In particular at 3 dpa the DBTT is shifted above 0 °C. ESPN does not define limits for the irradiated materials, but states that the effects of irradiation shall be taken into account in the design of the components; the use of more stringent design rules appears thus justified.

6. Design rules and corresponding stress limits

Design codes presented in Section 2 define specific rules to prevent the failure of components with respect to mechanical damage that might occur as a result of the imposed loadings. The mathematical expressions of these rules, as well as the corresponding limits, depend generally on the considered 'operating conditions'. These conditions (and the corresponding loadings) are classified into several categories based on the probability of occurrence and consequence of failure. To each category, a different "level"

Table 2
Minimum requirements on the ductility of the materials as defined by ESPN/RCC-MX and comparison with Eurofer97 properties in unirradiated/irradiated conditions.

	ESPN/RCC-MX Limit	Eurofer97 at BOL	Eurofer97 at 3 dpa
ε_t (RT)	>14%	22%	~14% (300 °C)
Toughness (0 °C)	>40 J	220 J	~200 J (300 °C) ~23 J (RT)
S_y/S_u (RT)	<0.85	0.83	0.92 (300 °C)

of criteria is then associated. In RCC-MX the rules to apply also depend on the ESPN classification of the component. For reasons of investment protection it has been decided to apply to TBM components the rules corresponding to the N1-class equipments even if less stringent rules could be used. Table 3 gives the correspondence between the loading categories as defined by the ITER Load Specifications and the different operating conditions and criteria levels as defined by SDC-IC and RCC-MX. In the following we will consider only Level A criteria since they are both the most conservative and comprehensive of all possible damage modes. Limits for Level C and Level D criteria are usually derived from those of Level A using lower safety factors.

In both codes, the aim of Level A criteria is to protect the component against the following damage modes:

(a) Immediate plastic collapse and plastic instability.
(b) Immediate plastic flow localisation.
(c) Local fracture due to exhaustion of ductility.
(d) Thermal creep.
(e) Ratcheting.
(f) Fatigue.
(g) Fast fracture.
(h) Buckling.

In the following chapters, design rules corresponding to each of these damage modes as defined by SDC-IC and RCC-MX will be discussed. In particular, damage modes (b) and (c) are characteristic of irradiated (or low ductility) materials where the potential of fracture modes with little or no plastic deformation increases (non-ductile damage modes). Damage modes (g) and (h) will not be considered in this paper. Several methods of analysis can be used to assess the behaviour of the components as recommended by the codes (elastic, inelastic, limit, experimental). We will only discuss rules to apply when elastic behaviour of the structure is assumed. Nomenclature will follow the conventions defined in SDC-IC since it seems more meaningful from ITER environment standpoint.

6.1. Criteria to prevent immediate plastic collapse and plastic instability

Immediate plastic collapse and immediate plastic instability are two modes of failure directly related to the primary stress intensity in the material: if a structure is loaded above the yield strength of the material, plastic deformation occurs until the structure collapses either because of excessive deformation or necking. Rules to prevent these modes of failure are essentially the same in SDC-IC and RCC-MX:

$$\begin{cases} \overline{P_m} \leqslant S_m \\ \overline{P_L + P_b} \leqslant k_{eff} S_m \\ \overline{P_L} \leqslant \min[1.5S_m, S_{y,\min}] \quad \text{(in local overlapping areas)} \\ \overline{P_L} \leqslant 1.1S_m \quad \text{(in local non overlapping areas)} \end{cases} \tag{3}$$

where P_m is the primary membrane stress, P_b the primary bending stress, P_L the local membrane stress, S_m the allowable stress and k_{eff} is a geometry and neutron dose dependant factor.

The main difference between SDC-IC and RCC-MX is in the definition of the k_{eff} coefficient which takes into account the increased bending moment capability of an elasto-plastic material with respect to an elastic-brittle material. In RCC-MX the value of k_{eff} is independent of the irradiation dose: $k_{eff} = k$ ($k = 1.5$ for rectangular sections). In SDC-IC, k_{eff} is assumed to be dependent on the dose so that comparable safety factors are maintained when the work-hardening capability of the material is reduced by neutron irradiation. This correction is not needed for Eurofer97 since, contrary to 316L(N)-IG, $1.5S_m$ falls in the elastic part of the stress–strain curve of the material.

The definition of S_m is also slightly different in SDC-IC and RCC-MX:

$$S_m = \begin{cases} \min\left[\frac{1}{3}S_{u,\min}(RT), \frac{1}{3}S_{u,\min}(T), \frac{2}{3}S_{y,\min}(RT), \frac{2}{3}S_{y,\min}(RT)\right] & (\text{SDC} - \text{IC}) \\ \min\left[\frac{1}{2.7}S_{u,\min}(RT), \frac{1}{2.7}S_{u,\min}(T), \frac{2}{3}S_{y,\min}(RT), \frac{2}{3}S_{y,\min}(RT)\right] & (RCC - MX) \end{cases} \tag{4}$$

In SDC-IC the value of S_m is also dependent on the neutron flux: for irradiation-hardening materials however this dependence can be neglected. Overall, RCC-MX definition leads to slightly higher values, as shown in Fig. 10.

6.2. Criteria to prevent failure against non-ductile damage modes

Primary stresses being limited by S_m, conventional design codes rely on sufficient ductility of the materials to simplify the analyses, ignoring secondary and peak stresses (apart from their effect on cyclic loadings like ratcheting and fatigue) since they are intrinsically self-limiting and cannot cause, by themselves, the failure of the structure. When the ductility of the material is reduced (intrinsically or because of neutron irradiation), it is however necessary to insure that the combined strain due to primary plus secondary stresses does not exceed the remaining elongation of the material. Moreover, because of elastic follow-up effects, the distinction between primary and secondary stresses becomes difficult.

SDC-IC defines two different modes of potential failure due to the limited ductility of the materials: immediate plastic flow localisation (which is closely tied to the loss of uniform elongation) and immediate local fracture due to exhaustion of ductility (which is associated with a low total elongation). Given that irradiated Eurofer97 retains considerable ductility after necking, as is shown by the high values of the total elongation and reduction of area, the latter is not an issue. Immediate plastic flow localisation is instead a concern for Eurofer97 [53].

To prevent failure against plastic flow localisation, SDC-IC and RCC-MX introduce the following criteria:

$$\overline{P_L + Q_L} \leqslant S_e \tag{5}$$

$$\overline{P_L + Q_L} \leqslant S_{em}^A \tag{6}$$

Table 3
Category conditions and corresponding criteria levels as defined by SDC-IC and RCC-MX.

Loading Category (According to ITER LS)	SDC-IC		RCC-MX	
	Category condition	Criteria level	Category condition	Criteria level
I Operational loading	Normal	A	SF1	A
II Likely loading	Upset	A	SF2	A
III Unlikely loading	Emergency	C	SF3	C
IV Extremely unlikely loading	Faulted	D	SF4	D

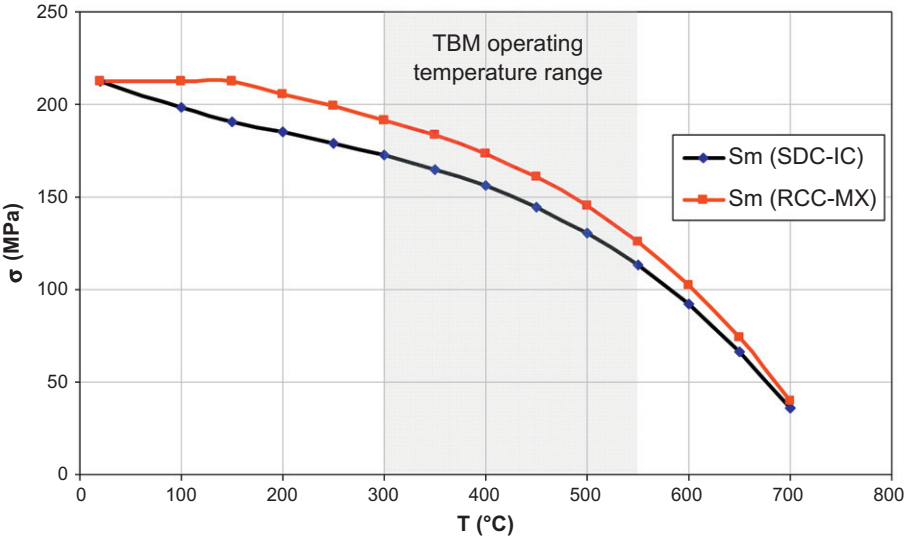

Fig. 10. Values of S_m calculated according to SDC-IC and RCC-MX for Eurofer97.

where Q_L is the secondary local membrane stress. SDC-IC defines S_e as:

$$S_e = \begin{cases} \frac{1}{3}[S_{u,\min}(T,\Phi t) + \frac{1}{2}\frac{E}{r_1}(\varepsilon_u(T,\Phi t) - 0.02)], & \varepsilon_u \geqslant 2\% \\ \frac{1}{3}S_{u,\min}(T,\Phi t), & \varepsilon_u < 2\% \end{cases} \quad (7)$$

RCC-MX defines S^A_{em} as:

$$S^A_{em}(T,\Phi t) = \frac{1}{2.5}\left\{\frac{r}{r+1}S_{u,\min}(T,\Phi t) + \frac{E}{r+1}\varepsilon_u(T,\Phi t)\right\} \quad (8)$$

where Φt is the cumulated neutron fluence (or dpa damage) and r_1 and r are the elastic follow-up factors, for which SDC-IC recommends a value of 4, while RCC-MX recommends a value of 3.

According to the previous definitions, values of S_e and S^A_{em} have been calculated using Eurofer97 irradiated properties at 300° and are shown in Fig. 11. In both cases, the initial steep decline of the allowable stress is due to the rapid decrease of the uniform elongation of the material with the irradiation dose. Once the saturation value of the uniform elongation is attained, the subsequent increase is due to the increase of the ultimate tensile strength. However, since limits apply throughout the lifetime of the component, no advantage should be taken on the increase of the ultimate tensile strength with irradiation dose and the allowable stress shall in this case be assumed equal to the minimum value calculated during the component lifetime. In case of TBMs, the minimum value (~200 MPa for both codes) is attained at saturation of the uniform elongation. This is also shown in Fig. 11.

Assuming:

- the values calculated at 300 °C as conservative in the range 20–350 °C;
- no effects of neutron irradiation on ductility and strength properties above 500 °C;
- interpolated values in the range 350–500 °C,

the allowable primary plus secondary membrane stress intensities at a neutron dose of 3 dpa are shown in Fig. 12. In case of SDC-IC, the definition of S_e takes no advantage on the residual uniform elongation of the material when its value is below 2%. For Eurofer97 $\varepsilon_u < 2\%$ for $T > 400$ °C, and the definition of S_e gives then the same values of S_m, the decrease above 400 °C corresponding to the decrease of S_u with temperature. This equates to considering all membrane stresses as primary, which is overly conservative.

In case of RCC-MX, the S^A_{em} limit increases above 300 °C up to a value of ~340 MPa at 500 °C corresponding to $\varepsilon_u \cong 1\%$ and $S_u \cong 400$ MPa. The minimum value (~170 MPa) is obtained at $T = 600$ °C for $\varepsilon_u \cong 0.5\%$ and $S_u \cong 280$ MPa, the subsequent increase corresponding to the increase of ε_u with temperature (Fig. 2).

In any case, limits defined by SDC-IC are considerably lower that those defined in RCC-MX, especially at 500 °C which corresponds to the average operating temperature of the TBM FW.

6.3. Criteria related to creep damage

Given the operating temperatures of most of TBM components (especially the FW), creep damage will have to be taken into account in the design. In order to guard against creep failure, the following limits need to be satisfied:

$$\Omega\overline{P_m} \leqslant S_t(T_{\max}, t) \quad (9)$$

$$\overline{P_L + \frac{P_b}{K_t}} \leqslant S_t(T_{\max}, t) \quad (10)$$

where t is the operating period corresponding to Level A and C loadings, $T_{\max}$ is the maximum operating temperature, S_t is the allowable stress intensity at time t and temperature $T_{\max}$ obtained from Fig. 6.

The factor Ω in Eq. (9) is introduced to take into account the effect of local membrane stresses as well as multiaxial stress states; if all membrane stresses can be classified as primary general membrane stresses then $\Omega = 1$; if not, then $\Omega = \Omega_1 \cdot \Omega_2$, where:

$$\Omega_1 = 1 + 0.2\left(\frac{\overline{L_m}}{\overline{P_m}}\right) = 1 + 0.2\left(\frac{\overline{P_L - P_m}}{\overline{P_m}}\right) \quad (\overline{P_L} > \overline{P_m}) \quad (11)$$

and Ω_2 is calculated as the ratio between the greatest tensile stress component of the primary principal stress tensor and the membrane stress $\overline{P_m}$ ($\Omega_2 > 1$). It should be noted that SDC-IC assumes $\Omega = 1$ and thus RCC-MX rules are generally more conservative.

Eq. (9) and the first of Eq. (3) are usually associated in order to define the S_{mt} limit as the allowable time-dependant primary membrane stress intensity on the basis of the operating time of the component (Fig. 13). The foreseen operating time in the ITER D-T phase of TBM components is about 850 h (3000 cycles/year, 2.5 years of operation, 400s plasma duration per pulse). It can be seen that, in the range of operating temperatures of TBM components, the limit for creep damage is not binding.

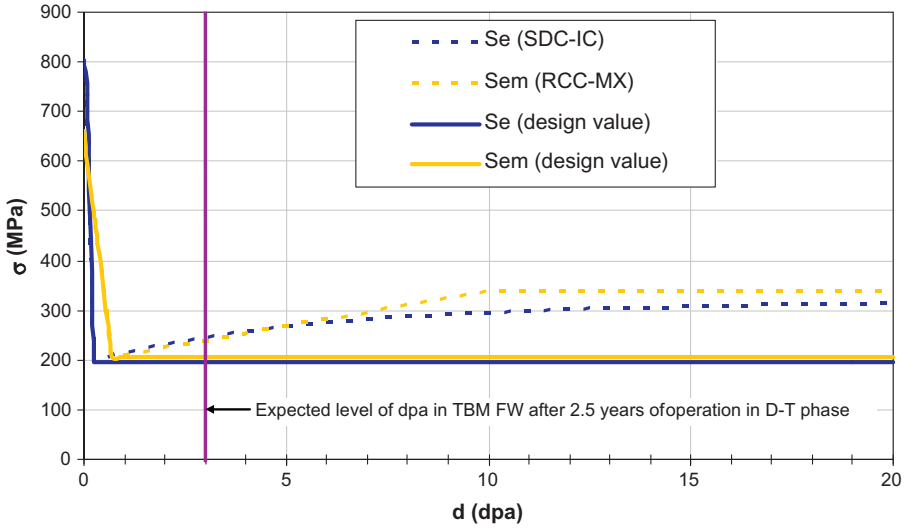

Fig. 11. Limit for primary plus secondary membrane stress intensity for Eurofer97 as calculated according to SDC-IC and RCC-MX definitions – values calculated at 300 °C.

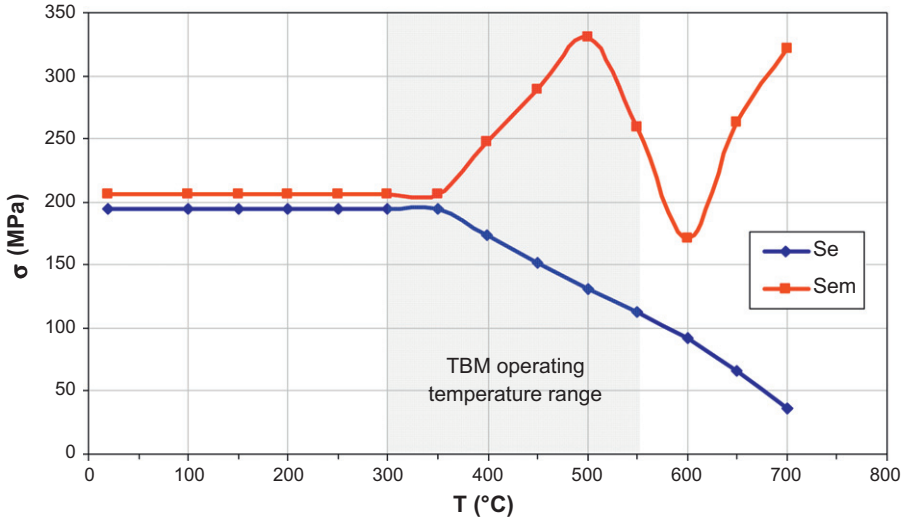

Fig. 12. Limit for primary plus secondary membrane stress intensity for Eurofer97 as a function of temperature at 3dpa.

However, when there is a risk of elastic follow-up as is the case for Eurofer97, membrane stresses from all sources should be included in Eq. (9). In this case Eq. (9) would become:

$$\overline{P_m + Q_m} \leqslant S_t(T_{\max}, t) \tag{12}$$

The same construction used for S_{mt} can in this case be repeated including the S_e and S^A_{em} limits (Eqs. (7) and (8)) as is shown in Fig. 14. In case of SDC-IC this introduces no additional requirements on the design of the component (since $S_e = S_m$ for Eurofer97, cf. Section 6.2), but gives much more stringent limits in case of RCC-MX. This approach is however very conservative and needs to be confirmed.

6.3.1. Creep usage fraction

Eqs. (9) and (10) are strictly applicable to cases in which the stress or temperature does not change significantly during the lifetime of the component. The creep usage fraction (U_t) provides a mean of generalising the use of S_t to cases in which the stress or temperature depend on time. It is defined as:

$$U_t = \sum_{j=1}^{n} \frac{t_j}{t_{s,j}} \tag{13}$$

and can be calculated by the following procedure:

- the total operating time is divided in N intervals in which the temperature and stress are approximately constant.
- For each interval j ($j = 1, \ldots, N$) of duration t_j, the highest operating temperature T_j and the highest stress intensity $\overline{\sigma_j}$ are calculated.
- The maximum operating time $t_{s,j}$ at temperature T_j and stress $\overline{\sigma_j}$ are obtained from the S_t curves (Fig. 6).

Eqs. (9) and (10) can then be generalised as:

$$U_t(\Omega\overline{P_m}) \leqslant 1 \tag{14}$$

$$U_t\left(\overline{P_L + \frac{P_b}{K_t}}\right) \leqslant 1 \tag{15}$$

6.3.2. Accounting for irradiation effects on creep damage

In RCC-MX it is recommended to replace S_t by $0.1S_t$ in Eqs. (9) and (10) (or 1 by 0.1 in Eqs. (14) and (15)). This would of course introduce much more stringent limits on the design of the component. It is however clearly stated that this rule applies only to

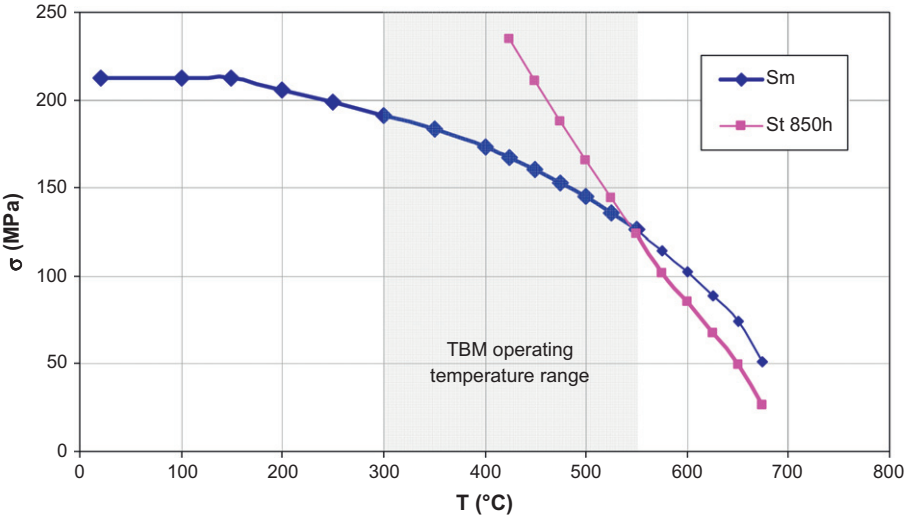

Fig. 13. Construction of the S_{mt} limit for Eurofer97.

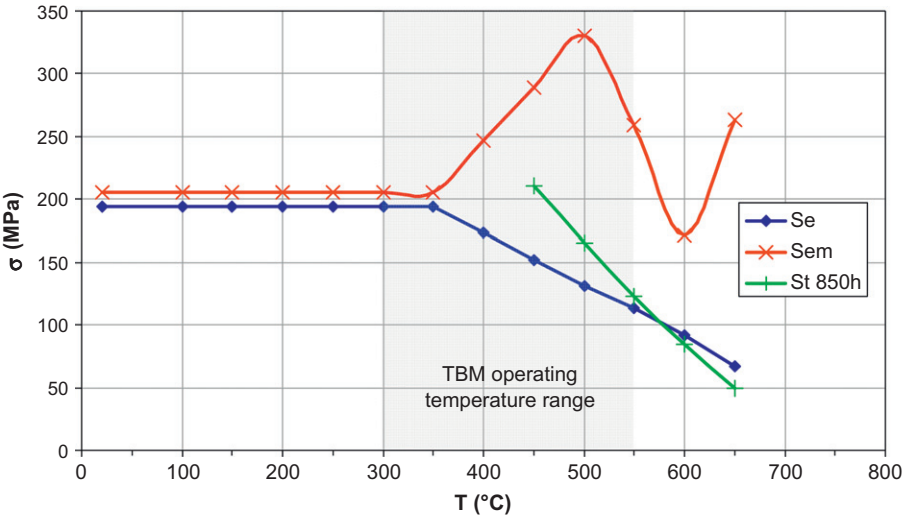

Fig. 14. Limit for creep damage including primary and secondary membrane stress for Eurofer97.

austenitic steels. The applicability of this rule to Eurofer97 is questionable, especially since irradiation creep is not an issue.

6.3.3. High temperature rules

Creep damage causing, over time, an increase in the deformation of the materials, its effects need to be included in all damage modes where the driving phenomenon is the total accumulated strain (or strain range), namely ratcheting and fatigue. For this reasons both codes differentiate between low-temperature (negligible creep) and high-temperature (significant creep) rules. High-temperature rules are more relevant for TBMs operation.

6.4. Criteria to prevent ratcheting

Ratcheting is, by definition, the accumulation of plastic deformation in structures subjected to cyclic stressing with a non-zero primary stress. When a structure is subjected to cyclic loading, the structure may show signs of permanent deformation at the end of the first cycle. During subsequent cycles, two cases may arise:

(a) after a few cycles, the overall permanent deformation is stable. The subsequent structural response is elastic or elasto-plastic and progressive incremental inelastic deformation is absent.
(b) the permanent overall deformation continues to increase as every loading cycle induces additional deformation and the structure gradually changes from its original shape until it eventually collapses. This behaviour is called progressive deformation or ratcheting.

In the first case, if after the first cycles the behaviour of the material becomes elastic at every point in the structure, elastic shakedown is said to be achieved. If the behaviour of the material at steady state is instead a closed elasto-plastic loop, plastic shakedown is said to be achieved. The term overall elastic shakedown is also used in the case of a structure which undergoes shakedown and in which the plastic strain only appears in localised strain concentration zones. The behaviour of the structure is generally elastic and only strain concentration zones undergo (limited) hysteresis cycles.

6.4.1. Low temperature rules

Two set of different rules are defined either in SDC-IC and RCC-MX, the most conservative one being the well known '3Sm' rule:

$$(\overline{P_m + P_b})_{\max} + (\Delta\overline{P} + \overline{\Delta Q})_{\max} \leqslant 3S_m(T) \tag{16}$$

where $(\overline{P_m + P_b})_{\max}$ is the maximum steady stress intensity value of the sum of the primary membrane plus bending stress reached during the cycle, $\Delta(\overline{P} + \overline{Q})_{\max}$ is the maximum range of the cyclic primary plus secondary stress intensities. For TBMs during normal operation (excluding disruptions) primary cyclic stresses can be neglected and $\Delta(\overline{P} + \overline{Q})_{\max} = \overline{\Delta P}_{\max} + \overline{\Delta Q}_{\max} = \overline{\Delta Q}_{\max}$.

It is clear that the theoretical limit for which a material experiences no permanent deformation is S_y (the proportional limit). It can be shown that, for an elastic-perfectly-plastic material, shakedown is ensured if the sum in the left term of Eq. (16) does not exceed $2S_y$. In this case, shakedown will occur and a negligible amount of permanent deformation will be present. For an elasto-plastic material undergoing strain-hardening, the limit can be higher than $2S_y$: the amount of permanent deformation will in this case depend on the material properties.

The limit defined in Eq. (16) is not $2S_y$ but $3S_m$. For cyclic-hardening materials included in the codes, the value of $3S_m$ is higher than $2S_y$ and the $3S_m$ rule ensures in this case either elastic shakedown or overall elastic shakedown and thus a certain amount of overall permanent deformation (material dependant) is allowed. Eventually, the assumption of elastic behaviour is justified for the analyses, since elastic response is the condition for all load cycles subsequent to shakedown.

For the materials that show cyclic-softening instead, $3S_m \sim S_u$. Since $S_u < 2S_y$, there is an allowance for some cyclic softening. Indeed, for the cyclic-softening materials included in the codes, the $3S_m$ limit ensures either overall elastic shakedown or plastic shakedown, thus allowing a limited amount of permanent deformation (material dependant). In this case, the behaviour of the material during the loading/unloading cycles should not be considered as elastic. It should also be noted that the requirement that the overall permanent deformation is negligible is necessary to ensure that the fatigue criteria, which are based on tests conducted without progressive deformation, represent the behaviour of the structure. These assumptions will need to be verified for Eurofer97.

6.4.2. High temperature rules

Different rules are proposed in RCC-MX and SDC-IC to prevent high temperature ratcheting. SDC-IC defines several tests with different degrees of conservatism, mostly based on the Bree diagram low temperature ratcheting rules. Test A-2 can be applied in case of TBMs, where one of the stress extremes takes place at a temperature below the negligible creep curve (300 °C). The following quantities are introduced:

$$X = \frac{(\overline{P_L + \frac{P_b}{K_t}})_{\max}}{S^*_{y,\min}} \tag{17}$$

$$Y = \frac{\Delta(\overline{P} + \overline{Q})_{\max}}{S^*_{y,\min}} \tag{18}$$

where $(\overline{P_L + \frac{P_b}{K_t}})_{\max}$ is the maximum steady stress intensity value of the sum of the local primary membrane stress and primary bending stress divided by the creep bending shape factor reached during the cycle, and $S^*_{y,\min}(T)$ is the average of the minimum yield strengths evaluated at the minimum and maximum temperatures during the cycle.

The rule to verify is then:

$$X + Y \leqslant 1 \tag{19}$$

or:

$$\left(\overline{P_L + \frac{P_b}{K_t}}\right)_{\max} + \Delta(\overline{P} + \overline{Q})_{\max} \leqslant S^*_{y,\min}(T) \tag{20}$$

The approach used in RCC-MX to prevent ratcheting is instead based on the concept of the "effective primary stress" (P_{eff}), that is an equivalent stress that would give the same immediate deformation as the actual cycling load combination. Values of P_{eff} are determined experimentally. Limits are then defined in terms of this effective primary stress. Before obtaining the effective primary stress intensity, it necessary to calculate the relative variation of secondary stress in relation to the primary stress considered. This introduces the notion of secondary ratio (SR):

$$SR_1 = \frac{\overline{\Delta Q_{\max}}}{\max(\sigma_m)} \tag{21}$$

$$SR_2 = \frac{\overline{\Delta Q_{\max}}}{\max(\sigma_L + \sigma_b)} \tag{22}$$

$$SR_3 = \frac{\overline{\Delta Q_{\max}}}{\max\left(\sigma_L + \frac{\sigma_b}{K_t}\right)} \tag{23}$$

where

$$\max(\sigma_m) = \frac{1}{2}[\max(\overline{P_m}) + (\sigma_m)_N]$$

$$\max(\sigma_L + \sigma_b) = \frac{1}{2}[\max(\overline{P_L + P_b}) + (\sigma_L + \sigma_b)_N]$$

$$\max\left(P_L + \frac{P_b}{K_t}\right) = \frac{1}{2}\left[\max\left(\overline{P_L + \frac{P_b}{K_t}}\right) + \left(\sigma_L + \frac{\sigma_b}{K_t}\right)_N\right]$$

$(\sigma_m)_N$ designates the true stress corresponding to the elastic calculated stress $\max(\overline{P_m + Q_m})$ and can be obtained by the intersection of the monotonic stress–strain curve with the Neuber curve $\sigma\varepsilon = \frac{\max(\overline{P_m+Q_m})^2}{E}$, as shown in Fig. 15, $(\sigma_L + \sigma_b)_N$ designates the true stress corresponding to the elastic calculated stress $\max(\overline{P_L + P_b + Q_m})$ and can be obtained by the intersection of the monotonic stress–strain curve with the Neuber curve $\sigma\varepsilon = \frac{\max(\overline{P_L+P_b+Q_m})^2}{E}$, with the same construction shown in Fig. 15 and $\left(\sigma_L + \frac{\sigma_b}{K_t}\right)_N$ designates the true stress corresponding to the elastic calculated stress $\max\left(\overline{P_L + \frac{P_b}{K_t} + Q_m}\right)$ and can be obtained by the intersection of the monotonic stress–strain curve with the Neuber curve $\sigma\varepsilon = \frac{\max(\overline{P_L+\frac{P_b}{K_t}+Q_m})^2}{E}$, with the same construction shown in Fig. 15.

Once the values of the secondary ratios known, the corresponding effective primary stresses can be obtained by means of the efficiency diagram (Fig. 16) as:

$$P_1 = \frac{\max(\sigma_m)}{V_1} \tag{24}$$

$$P_2 = \frac{\max(\sigma_L + \sigma_b)}{V_2} \tag{25}$$

$$P_3 = \frac{\max\left(\sigma_L + \frac{\sigma_b}{K_t}\right)}{V_3} \tag{26}$$

where V_1, V_2, V_3 are the efficacy indexes obtained from SR_1, SR_2 and SR_3 using the efficiency diagram. The following limits need then to be verified:

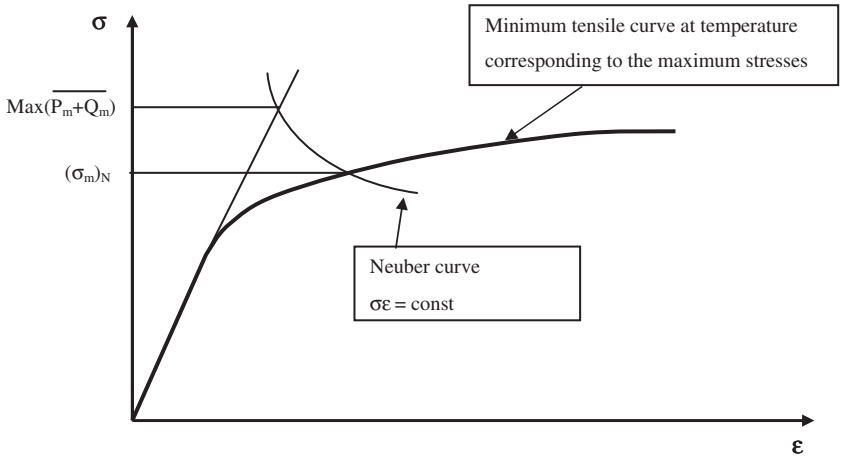

Fig. 15. Determination of $(\sigma_m)_N$ using Neuber's rule.

$$P_1 \leqslant 1.3S_m(T) \tag{27}$$

$$P_2 \leqslant 1.5 \times 1.3S_m(T) \tag{28}$$

(a) the plastic strain + associated creep strain at a stress of $1.25 \times P_1$ should not exceed 1%,
(b) the plastic strain + associated creep strain at a stress of $1.25 \times P_3$ should not exceed 2%.

The plastic strain can be determined from the average monotonic stress–strain curve as shown in Fig. 15 while the creep strain can be obtained directly by the creep laws.

A direct comparison of the two methodologies (SDC-IC/RCC-MX) is not straightforward. By limiting the allowable primary plus secondary stress intensity to S_y, rule (20) effectively prevents ratcheting from occurring, while creep strain is limited by Eqs. (14) and (15). This is however true only for a cyclic-hardening material: in order to maintain the same degree of conservatism for a cyclic softening material, the values of S_y should theoretically be calculated on the reduced cyclic stress–strain curve. Limiting the allowable stress to S_y (instead of the theoretical $2S_y$ limit) leaves however a considerable margin for cyclic softening and is already very conservative.

The efficiency index method in RCC-MX is, in theory, less conservative than Eq. (20), since it allows a certain degree of permanent deformation to occur. Indeed, for austenitic-type steels, $1.3S_m = 1.3 \times 0.9S_y = 1.17S_y$. Limiting the primary effective membrane stress to $1.3S_m$ leads then to a certain degree of permanent plastic strain (less than 1% for 316L(N)-IG). For Eurofer97, however, $1.3S_m = 1.3 \times (S_u/2.7) = 0.48S_u < S_y$. The effective primary membrane stress is then limited to a value lower than the proportional limit and according to the definition, no plastic deformation is allowed. For Eurofer97, the efficacy index method can yield more conservative result than the $3S_m$ rule. On the other hand, limiting the accumulated thickness-averaged plastic strain to 1% (and the bending strain to 2%) could be too permissive for Eurofer97, which at 500 °C already shows values of the uniform elongation close to 1% and as low as 0.2% after few dpa at 300 °C. A possible approach could be in this case to limit the primary effective membrane stress to S_y (thus insuring no permanent plastic deformation) and apply more conservative limits for the creep strain. However, since the basis for the efficacy index method is experimental, this approach needs to be confirmed.

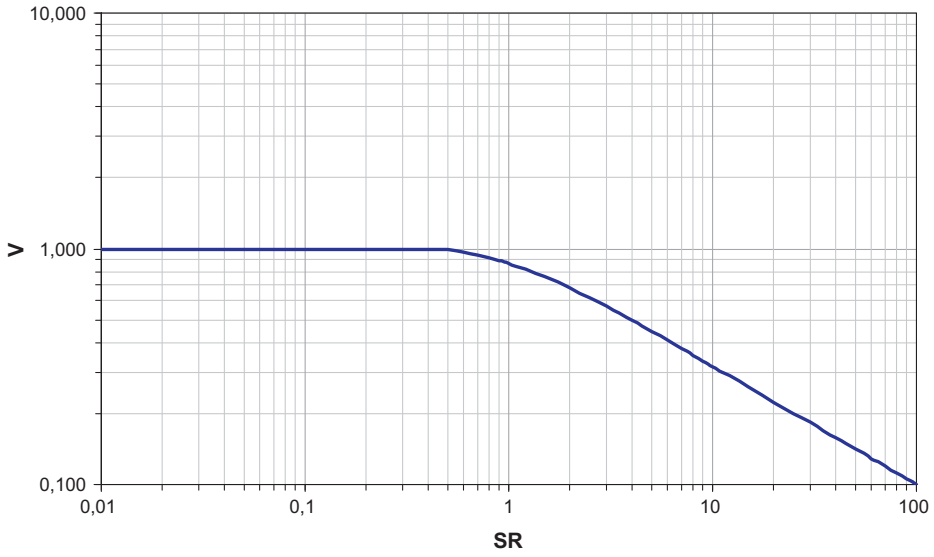

Fig. 16. Efficiency diagram.

The prediction of ratcheting in cycling-softening materials, especially when taking into account the interactions with fatigue and creep damage, is indeed a very complex subject. The RCC-MX approach is based on the results of several experimental tests performed on different geometries and materials: the efficiency diagram represents a lower bound to the results of these experimental tests. Theoretical/computational approaches are possible, and several elasto-visco-plastic models have been proposed in the past to simulate the evolution of damage in structures subjected to cyclic loadings [54,55]. Some of these models have been adapted and identified on Eurofer97 [56,57]: FE simulation under TBM-relevant geometries and operating conditions have been performed in order to assess the degree/lack of conservatism of the rules contained in the codes [58,59]. The obtained results seem to indicate that limits defined by the codes are already very conservative.

The discussion of these models is beyond the scope of this paper: because of the high computational times, analyses are usually limited to simple FE meshes. They could however be useful for local analyses in zones where there is a concern related to the applicability of the rules contained in the codes.

6.5. Criteria to prevent fatigue damage

Criteria to estimate the allowable number of cycles a component can withstand (N_f) are based on the use of the fatigue design curve as defined in Section 4.3. Assuming that the cycles are all the same, N_f can be calculated once the total strain range intensity ($\overline{\Delta\varepsilon_{tot}}$) during a cycle is known. Elastic analysis, however does not allow a direct estimation of the total strain range, since the effects of plasticity above the yield point are not accounted for.

The procedure used to estimate the total strain range intensity is essentially the same in SDC-IC and RCC-MX; the total strain range is expressed as:

$$\overline{\Delta\varepsilon_{tot}} = \overline{\Delta\varepsilon_{el+pl}} = \overline{\Delta\varepsilon_1} + \overline{\Delta\varepsilon_2} + \overline{\Delta\varepsilon_3} + \overline{\Delta\varepsilon_4} \tag{29}$$

where

- $\overline{\Delta\varepsilon_1}$ is the elastic component of the total strain range. It can be calculated for the total stress intensity range according to:

$$\overline{\Delta\varepsilon_1} = \frac{2}{3}\frac{(1+\nu)}{E}\overline{\Delta\sigma_{tot}} \tag{30}$$

- $\overline{\Delta\varepsilon_2}$ represents the increase in the plastic strain range caused by cyclic primary stresses (if present). It can be calculated on the basis of the equivalent primary cyclic stress range ($\overline{\Delta P_{eff}} = \overline{\Delta[P_m + 0.67(P_b + P_L - P_m)]}$) using the cyclic stress–strain curve at the maximum temperature reached during the cycle. Its value however is usually negligible, especially in the case of TBMs where primary cyclic stresses can be neglected during normal operation.
- $\overline{\Delta\varepsilon_3}$ represents the plastic strain measured on the cyclic stress–strain curve of the material at the maximum temperature reached during the cycle. Its value is given by the intersection of the cyclic stress–strain curve with the Neuber curve $\overline{\Delta\sigma}\cdot\overline{\Delta\varepsilon} = \overline{\Delta\varepsilon_1}\overline{\Delta\sigma_{tot}}$ (when $\overline{\Delta\varepsilon_2} = 0$). It is calculated by means of the K_ε coefficient according to:

$$\overline{\Delta\varepsilon_3} = (K_\varepsilon - 1)\overline{\Delta\varepsilon_1} \quad (\overline{\Delta\varepsilon_2} = 0) \tag{31}$$

  Values of K_ε can be obtained from the cyclic stress strain curves. They have been calculated for Eurofer97 and are shown in Fig. 17.

- $\overline{\Delta\varepsilon_4}$ represents the increase because of triaxiality effects. It is calculated by means of the K_v coefficient according to:

$$\overline{\Delta\varepsilon_4} = (K_v - 1)\overline{\Delta\varepsilon_1} \quad (\overline{\Delta\varepsilon_2} = 0) \tag{32}$$

  Values of K_v can be obtained from the cyclic stress strain curves. They have been calculated for Eurofer97 and are shown in Fig. 18.

6.5.1. Fatigue usage fraction

The notion of the fatigue usage fraction has been introduced in the codes to generalise the use of the fatigue curve to components that experience different type of cycles during their operating period. The fatigue usage fraction (V) is calculated according to following procedure:

- the operating period is divided into M types of cycles;
- for each cycle of type j (j = 1 to M), the corresponding number of cycles n_j the component has to withstand is calculated;
- for each cycle of type j (j = 1 to M), the corresponding total strain range $\overline{\Delta\varepsilon_j}$ is calculated;
- when one ore more types of strain cycles separately produce strain ranges lower than those which would be obtained with a single type of cycle formed by the succession of these cycles, they must be combined according to rules given by the codes;
- the number of allowable cycles N_j under a total strain range $\overline{\Delta\varepsilon_j}$ is estimated on the fatigue design curve;

The fatigue usage fraction is then given by:

$$V = \sum_{j=1}^{M} V_j = \sum_{j=1}^{M} \frac{n_j}{N_j} \tag{33}$$

Criteria are verified if the cumulative fatigue usage fraction is less than 1:

$$V \leqslant 1 \tag{34}$$

6.5.2. Creep–fatigue interaction

No rules are yet given in SDC-IC for the estimation of the fatigue lifetime of the component at temperatures where creep effects are relevant. Given their operating temperature range, this is a concern for Eurofer97 structures in TBMs.

In RCC-MX, rules to estimate damage resulting from the accumulation of the effects of creep and fatigue are based on the use of the fatigue usage fraction (V) as defined in Section 6.5.1 and the creep rupture usage fraction (W) which is calculated using the same procedure described in Section 6.3.1 for the creep usage fracture, but using, instead of the S_t curve, the S_r curve, S_r being the minimum creep rupture stress.

In the calculation of the fatigue usage fraction, the value of the total strain range must however be corrected for the effects of creep:

$$\overline{\Delta\varepsilon_{tot}} = \overline{\Delta\varepsilon_{el+pl}} + \overline{\Delta\varepsilon_{fl}} = (\overline{\Delta\varepsilon_1} + \overline{\Delta\varepsilon_2} + \overline{\Delta\varepsilon_3} + \overline{\Delta\varepsilon_4}) + \overline{\Delta\varepsilon_{fl}} \tag{35}$$

The value of $\overline{\Delta\varepsilon_{fl}}$ can be obtained starting from the 'real' stress $\overline{\Delta\sigma^*}$ measured on the cyclic stress–strain curve at the strain $\overline{\Delta\varepsilon_{el+pl}}$ calculated as explained in Section 6.5. The following quantities need to be estimated:

- the highest temperature during the holding time T: θ^*;
- the period for which the temperature of the component exceeds the temperature at which the creep effects appear: T^*;
- the symmetrisation coefficient K_s, obtained as function of the ratio $\overline{\Delta\sigma^*}/2S_{y,\min}(\theta^*)$. A value of K_s = 0.5 can be assumed for Eurofer97 at 500 °C.
- the average value of the primary equivalent stress during the cycle:

$$\mathrm{Moy}\overline{P} = \frac{1}{T}\int_0^T \overline{[P_m + 0.66(P_L + P_b - P_m)]}dt \tag{36}$$

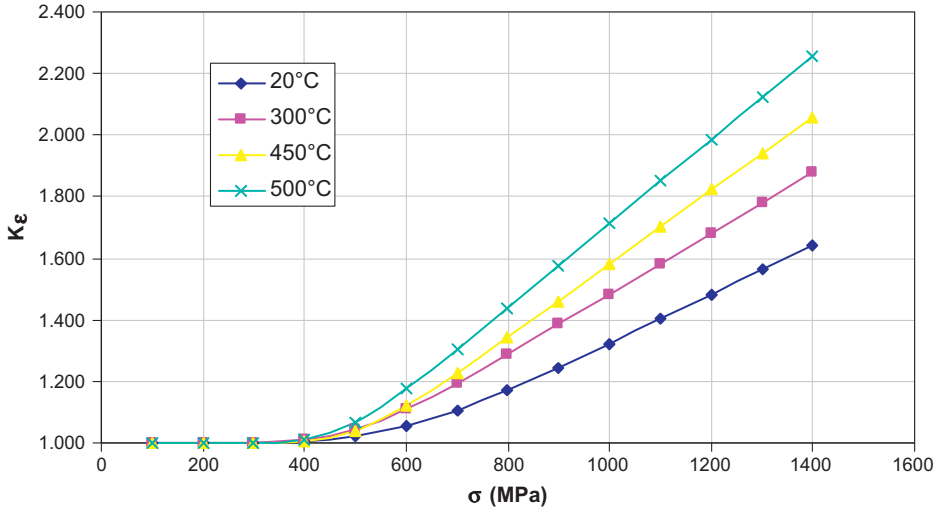

Fig. 17. Values of K_ε at different temperatures for Eurofer97.

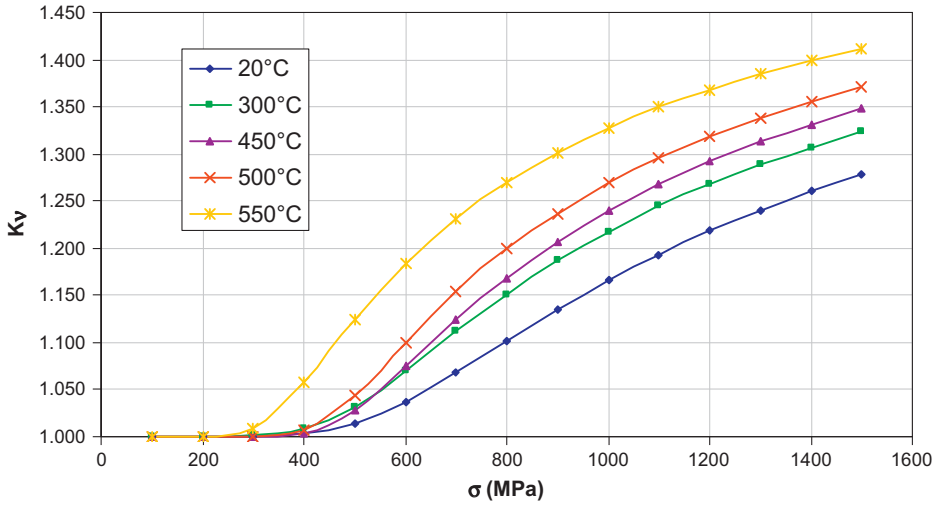

Fig. 18. Values of K_v at different temperatures for Eurofer97.

The value of $\overline{\Delta\varepsilon_{fl}}$ is then the creep strain due to the stress $\sigma_k = \mathrm{Moy}\overline{P} + K_s\overline{\Delta\sigma^*}$ applied for a time T^*; this can be obtained from the creep strain law at a temperature θ^*. Once the total strain range intensity corrected for the effects of creep is known for each of the cycles, the fatigue usage fraction and the creep rupture usage fraction can be calculated as:

$$V_A = \sum_{j=1}^{K} V_j(\overline{\Delta\varepsilon}_{tot\,j}) \quad ; \quad W_A = \sum_{j=1}^{K} W_j\left(\frac{\sigma_{k,j}}{0.9}, \theta^*\right) \tag{37}$$

Criteria are then verified if the point defined by the coordinates (V_A, W_A) falls within the allowable area defined by the creep–fatigue interaction diagram given in the codes.

6.5.3. Effects of irradiation

When irradiation is significant, the procedure described in Section 6.5 should be applied on the irradiated cyclic stress–strain curve. However, in the case of Eurofer97 and for temperatures above 400 °C, the unirradiated values can be used.

For temperatures below 400 °C, when there is a significant loss of ductility, a correction factor for the total strain range can be introduced on the fatigue design curve based on the ratio between the minimum unirradiated instantaneous ductility and the minimum irradiated instantaneous ductility:

$$fi_j = \left(\frac{(\varepsilon_{tr})_u}{(\varepsilon_{tr})_i}\right)_j^c \tag{38}$$

where

$$\varepsilon_{tr} = \ln\left(\frac{100}{100 - \%RA}\right) \tag{39}$$

However, as stated in Section 4.3.1, the simultaneous effects of irradiation and fatigue are different from those measured on post-irradiation samples and additional work is needed to harmonise design rules and material data.

As for the effects of irradiation on the fatigue creep-interaction, RCC-MX recommends multiplying the creep rupture usage fraction (cf. Section 6.5.2) by a factor 10. This rule however applies only to austenitic steels.

7. Conclusions

This paper gives an overview of the issues related to the design of Eurofer97 structures for TBMs components. Currently it appears

that there is no unique set of C&S covering all requirements for TBMs design. The next edition of the RCC-MR (RCC-MRx) will however include specific design rules for irradiated components and could also include Eurofer97 mechanical properties data and specific manufacturing techniques for TBMs components. It could in this case be used as the sole C&S for TBMs design.

With the recent availability of new data concerning fatigue, creep and irradiation induced changes in material properties, the characterisation of Eurofer97 is at least to the level of other 9Cr steels considered in nuclear design codes. With respect to the design of Eurofer97 structures, the main issue is the reduced ductility of the material when compared to austenitic steels (or even other 9Cr steels used in the nuclear industry). In the absence of irradiation damage, Eurofer97 already shows very limited uniform elongation which drops sharply after a few fraction of dpa. Even if the effects of irradiation are limited above 400 °C, the BOL properties justify the use of additional design criteria to prevent failure of the components. Design rules contained in present-day codes have however been developed mainly for austenitic steels (like the 316L(N)-IG steel grade used for the ITER blanket). Their applicability/degree of conservatism for Eurofer97 structures need to be confirmed by more experimental tests. In particular, design rules concerning non-ductile damage modes as well as the concurrent effects of high temperature operation (significant creep), fatigue and irradiation damage need to be further investigated.

Acknowledgements

This work was performed by the TBM Consortium of Associates in support of design activities carried out in the framework of Fusion for Energy TBMs development. The views and opinions expressed herein do not necessarily reflect those of the European Commission.

References

[1] R. Andreani, E. Diegele, W. Gulden, R. Laesser, D. Maisonnier, et al., Fusion Eng. Des. 81 (2006) 25–32.
[2] D. Maisonnier, I. Cook, P. Sardain, L.V. Boccaccini, L. Di Pace, Fusion Eng. Des. 81 (2006) 1123–1130.
[3] R. Andreani, E. Diegele, R. Laesser, B. van der Schaaf, J. Nucl. Mater. 329–333 (2004) 20–30.
[4] B. van der Schaaf, F. Tavassoli, C. Fazio, E. Rigal, E. Diegele, et al., Fusion Eng. Des. 69 (2003) 197–203.
[5] L. Giancarli et al., Fusion Eng. Des. 81 (2006) 393–405.
[6] L.V. Boccaccini et al., Fusion Eng. Des. 84 (2) (2009) 333–337.
[7] E.E. Bloom, J. Nucl. Mater. 258–263 (1998) 7–17.
[8] A.A.F. Tavassoli, J. Nucl. Mater. 302 (2002) 73–88.
[9] The Pressure Equipment Directive, PED 97/23/EC: <http://ec.europa.eu/enterprise/sectors/pressure-and-gas/documents/ped/>.
[10] Arrêté du 12 décembre 2005 relatif aux équipements sous pression nucléaires, NOR: INDI0506414A, Rev. 22/1/2009: <http://www.legifrance.gouv.fr/WAspad/UnTexteDeJorf?numjo=INDI0506414A>.
[11] Arrêté du 10 août 1984 relatif à la qualité de la conception, de la construction et de l'exploitation des installations nucléaires de base: <http://www.legifrance.gouv.fr/affichTexte.do?cidTexte=JORFTEXT000000321244&dateTexte=20101104>.
[12] V. Barabash, G. Sannazzaro, N. Mitchell, C. Jong, B. Giraud et al., Codes and Standards and regulation issues for design and construction of the ITER mechanical components, Fusion Engineering and Design, in press. doi:10.1016/j.fusengdes.2010.03.021.
[13] S. Majumdar, P. Smith, Fusion Eng. Des. 41 (1998) 25–30.
[14] A.A.F. Tavassoli, F. Touboul, J. Nucl. Mater. 233–237 (1996) 51–61.
[15] Guide for ASME Stamp Holders, Use of ASME Sec. VII, Div 1 to Meet the EC Pressure Equipment Directive (97/23/EC), ASME, July 2, 2001.
[16] A.A.F. Tavassoli, A. Alamo, L. Bedel, L. Forest, J.-M. Gentzbittel, et al., J. Nucl. Mater. 329–333 (2004) 257–262.
[17] G. Aiello, F. Gabriel, A. Li-Puma, A. Pajot, G. Rampal, et al., Fusion Eng. Des. 85 (2010) 1565–1572.
[18] F. Cismondi, S. Kecskes, G. Aiello, HCPB TBM thermo mechanical design: assessment with respect codes and standards and DEMO relevancy, in: Presented at the 26th Symposium On Fusion Technology (SOFT-26), Fusion Engineering and Design, in press, doi:10.1016/j.fusengdes.2011.02.067.
[19] Design and Construction for Mechanical Components of FBR nuclear islands (RCC-MR), AFCEN, 2007 edition.
[20] G.M. Kalinin, B.S. Rodchenkov, V.A. Pechenkin, J. Nucl. Mater. 329–333 (2004) 1615–1618.
[21] Règles de conception et de construction des matériels mécaniques des réacteurs expérimentaux de leurs auxiliaires et des dispositifs d'irradiation (RCC-MX), CEA Edition 2008.
[22] Y. Poitevin, L.V. Boccaccini, M. Zmitko, I. Ricapito, J.-F. Salavy, et al., Fusion Eng. Des. 85 (2010) 2340–2347.
[23] V.A. Chuyanov, D.J. Campbell, L.M. Giancarli, Fusion Eng. Des. 85 (2010) 2005–2011.
[24] D.S. Gelles, J. Nucl. Mater. 239 (1996) 99–106.
[25] S.J. Zinkle, N.M. Ghoniem, Fusion Eng. Des. 51–52 (2000) 55–71.
[26] R. Lindau, A. Möslang, M. Schirra, Fusion Eng. Des. 61–62 (2002) 659–664.
[27] S. Majumdar, Fusion Eng. Des. 29 (1994) 158–163.
[28] E. Lucon, P. Benoit, P. Jacquet, E. Diegele, R. Lässer, et al., Fusion Eng. Des. 81 (2006) 917–923.
[29] N. Baluc et al., J. Nucl. Mater. 367–370 (2007) 33–41.
[30] E. Lucon, W. Vandermeulen, J. Nucl. Mater. 386–388 (2009) 254–256.
[31] B. van der Schaaf, C. Petersen, Y. De Carlan, J.W. Rensman, E. Gaganidze, X. Averty, J. Nucl. Mater. 386–388 (2009) 236–240.
[32] D.A. McClintock, M.A. Sokolov, D.T. Hoelzer, R.K. Nanstad, J. Nucl. Mater. 392 (2009) 353–359.
[33] A. Alamo, J.L. Bertin, V.K. Shamardin, P. Wident, J. Nucl. Mater. 367–370 (2007) 54–59.
[34] J. Rensman et al., J. Nucl. Mater. 329–333 (2004) 1113–1116.
[35] J. Rensman et al., J. Nucl. Mater. 307–311 (2002) 250–255.
[36] E. Lucon, M. Decréton, E. van Walle, Fusion Eng. Des. 69 (2003) 373–377.
[37] A. Alamo, M. Horsten, X. Averty, E.I. Materna-Morris, M. Rieth, J.C. Brachet, J. Nucl. Mater. 283–287 (2000) 353–357.
[38] P. Chiovaro, P.A. Di Maio, G. Vella, Fusion Eng. Des. 75–79 (November) (2005) 725–730.
[39] P. Fernandez et al., Fusion Eng. Des. 75–79 (2005) 1003–1008.
[40] G. Yu, N. Nita, N. Baluc, Fusion Eng. Des. (75–79) (2005) 1037–1041.
[41] Pierre Marmy, Tomas Kruml, J. Nucl. Mater. 377 (2008) 52–58.
[42] J. Aktaa, M. Lerch, J. Nucl. Mater. 353 (2006) 101–108.
[43] M. Walter, J. Aktaa, M. Lerch, Int. J. Fatigue 30 (2008) 568–573.
[44] Matthias Weick, J. Aktaa, J. Nucl. Mater. 367–370 (2007) 633–636.
[45] C. Petersen, A. Povstyanko, V. Prokhorov, A. Fedoseev, O. Makarov, M. Walter, J. Nucl. Mater. 386–388 (2009) 299–302.
[46] S.W. Kim, H. Tanigawa, T. Hirose, A. Kohayama, J. Nucl. Mater. 386–388 (2009) 529–532.
[47] T. Hirose, H. Tanigawa, M. Ando, A. Kohyama, Y. Katoh, M. Narui, J. Nucl. Mater. 307–311 (2002) 304–307.
[48] Pierre Marmy, J. Nucl. Mater. 367–370 (2007) 86–91.
[49] J. Bertsch, R. Lindau, A. Möslang, J. Nucl. Mater. 233–237 (1996) 276–279.
[50] R. Lindau, A. Möslang, J. Nucl. Mater. 212–215 (1994) 599–603.
[51] P. Marmy, B. M Oliver, J. Nucl. Mater. 318 (2003) 132–142.
[52] C. Petersen, D. Rodrian, Int. J. Fatigue 30 (2008) 339–344.
[53] R. Chaouadi, J. Nucl. Mater. 372 (2008) 379–390.
[54] G. Kang, Int. J. Fatigue 30 (2008) 1448–1472.
[55] J.L. Chaboche, Int. J. Plast 24 (2008) 1642–1693.
[56] J. Aktaa, R. Schmitt, Fusion Eng. Des. 81 (2006) 2221–2231.
[57] J. Aktaa, C. Petersen, Eng. Fract. Mech. 76 (2009) 1474–1484.
[58] R. Sunyk, J. Aktaa, J. Nucl. Mater. 367–370 (2007) 1404–1409.
[59] J. Aktaa, M. Weick, C. Petersen, J. Nucl. Mater. 386–388 (2009) 911–914.